Cite this: DOI: 10.1039/c0xx00000x

www.rsc.org/xxxxxx

COMMUNICATION

A novel ultra-thin catalyst layer based on wheatear-like catalysts for polymer electrolyte membrane fuel cells

Changkun Zhang [a, b], Hongmei Yu *[, a], Li Fu [a, b], Yuan Gao [a, b], Jia Jia [a, b], Shangfeng Jiang [a, b], Baolian Yi [a], Zhigang Shao [a,]

Received (in XXX, XXX) Xth XXXXXXXXX 20XX, Accepted Xth XXXXXXXXX 20XX
DOI: 10.1039/b000000x

The wheatear-like catalysts were prepared on the Co-OH-CO_3 nanowires to design an ultra-thin catalyst layer (UTCL). Without any ionomer, the UTCL exhibited a maximum power density of 481 mW cm^{-2} at ultra-low Pt loading of 43 μg cm^{-2}_{Pt}, resulting in a relatively high Pt utilization of 11.2 kW g^{-1}_{Pt}. It is expected that the nanostructured thin film materials will lead to further technological advancements in fuel cells and applications.

Currently, extensive research has been carried out to realize the ultimate solution to the world energy demands. Great expectations are held for technologies such as fuel cells and lithium-air batteries that rely on electrochemical processed. Polymer electrolyte membrane fuel cells (PEMFCs) stand out as one of the most promising candidates, as it ensures clean energy under commercially viable operating conditions. However, high cost is still one of the major challenges for commercialization of PEMFCs. In particular, one of the barriers is the high price and limited resource of platinum-based electrocatalysts which are widely used in PEMFCs[1]. Numerous investigations have been carried out to improve the activity and durability of Pt for oxygen reduction reaction (ORR) in PEMFCs[2, 3]. For instance, a series of binary Pt-M alloys with transition metals (M = Cr, Mn, Co, Ni) or dealloying of some alloys of Pt, as well as synthesis of platinum core-shell electrocatalyst, are routes to make Pt-based electrocatalysts more active than pure Pt electrocatalysts[4]. An alternative strategy employed is to introduce 1D material such as Ag[5], Cu[6], and Ni[7] nanowires (NWs) as the templates to from core-shell NWs electrocatalysts. Supportless Pt and PtPd nanotubes templated from Ag NWs, investigated by Yan and coworkers, showed a slightly higher mass activity and 3.1-times-higher specific activity than Pt/C[5]. And PtPdCu and PtCu alloy nanoparticle nanotubes were fabricated by Li et al using partially sacrificial Cu NWs as templates[6]. The self-supporting, 1D, noble-metal-based materials may be potential materials to prevent aggregation or Ostwald ripening problems. However, it has been realized that the efficient utilization of Pt electrocatalysts in PEMFCs not only relies on the intrinsic catalytic activity of these electrocatalysts, but also strongly depends on the structure of the catalyst layer (CL) built up by the electrocatalysts[8]. In the conventional CL, the 1D, supportless electrocatalysts or electrocatalysts on carbon powder have disordered structure which hinders the electron and proton transports, leading to a low Pt utilization efficiency. A unique nanostructured thin film (NSTF) electrode which consists of oriented nanometer-sized crystalline organic whiskers, can enhance specific activity of the electrocatalysts[9, 10]. In this regard, advanced CL that has high performance using ultra low platinum loading is in high demand for fuel cells application. Middelman firstly proposed the ordered CL concept that was supposed to be able to maximize the utilization of catalyst and enhance the transport of reactants, electrons, and protons[11]. Besides, carbon nanotubes (CNTs)[12-14], carbon coated tin[15], TiO_2 nanotube arrays[16-18] and polypyrrole nanowires[19] are attempted to form an ordered CL.

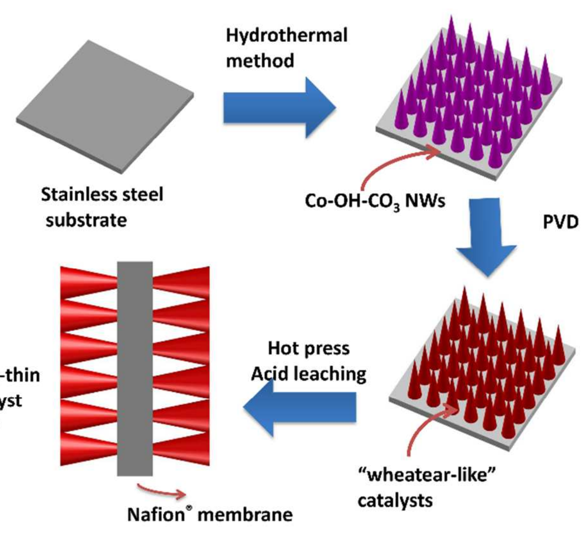

Figure 1 Illustration of the UTCL fabrication based on the Co-OH-CO_3 NWs.

Herein, we designed an ultra-thin catalyst layer (UTCL) with oriented 3D catalysts instead of conventional carbon based electrocatalysts. In the design, the key material is the 1D cobalt-hydroxide-carbonate (Co-OH-CO_3) nanostructures. The Co-OH-CO_3 NWs are usually taken as the precursor of Co_3O_4 and have been successfully synthesized on a variety of substrates including transparent conducting glass, nickel foil, nickel foam, Ti, and Fe-Co-Ni alloy[20-22]. In this work, we synthesized wheatear-like structure electrocatalysts using the Co-OH-CO_3 NWs as template. The fabricated UTCL exhibited enhanced performance at ultra-low Pt loading.

Figure 1 schematically illustrates the fabrication process of UTCL for PEMFCs. In this method, a simple hydrothermal method was employed to synthesize Co-OH-CO_3 NWs on the stainless steel substrate. Subsequently, Pd and Pt catalysts were deposited onto the Co-OH-CO_3 NWs by radio frequency (RF) magnetron sputtering system to form the Co-OH-CO_3-Pt and Co-OH-CO_3-PdPt electrodes. Then the catalysts coated Co-OH-CO_3 NWs film was transferred completely from stainless steel to both sides of Nafion membrane. Finally, the supportless Pt and PdPt catalysts were fabricated onto Nafion® membrane via immersing the electrode into 50mM H_2SO_4 solution to remove the Co-OH-CO_3 NWs template.

The chemical reactions involved in the preparation process of Co-OH-CO_3 NWs on the stainless steel can be illustrated as follows[21]:

$$Co^{2+} + xF^- \rightarrow CoF_x^{(x-2)-} \quad (1)$$

$$H_2NCONH_2 + H_2O \rightarrow 2NH_3 + CO_2 \quad (2)$$

$$CO_2 + H_2O \rightarrow CO_3^{2-} + 2H^+ \quad (3)$$

$$NH_3 \cdot H_2O \rightarrow NH_4^+ + OH^- \quad (4)$$

$$CoF_x^{(x-2)-} + 0.5(2-y)CO_3^{2-} + yOH^- + nH_2O \rightarrow Co(OH)_y(CO_3)_{0.5(2-y)} \cdot nH_2O + xF^- \quad (5)$$

At the beginning, Co^{2+} were coordinated with F^- to form $CoF_x^{(x-2)-}$ in the homogeneous solution. As the temperature ramped to 120°C, the hydrolysis-precipitation process of urea took place at around 70°C and a number of CO_3^{2-} and OH^- was formed gradually, which could help to release Co^{2-} slowly from $CoF_x^{(x-2)-}$ in the solution. When the concentration of CO_3^{2-} and OH^- anions in the solution increased, the further reaction led to the formation of a nucleus. The nucleus was prone to form on the stainless steel substrates' surface rather than in aqueous solution, F^- in the solution has played a crucial role throughout the preparation process.[21, 23]

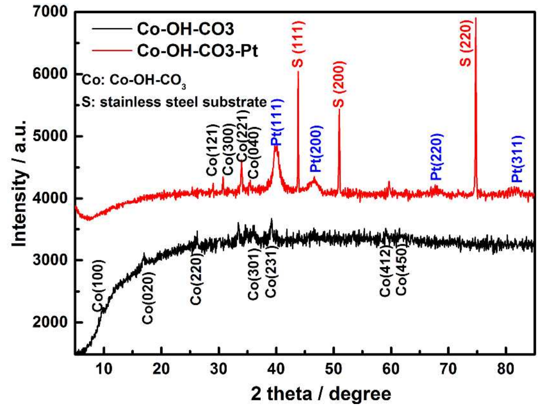

Figure 2 The XRD patterns of the Co-OH-CO_3 and Co-OH-CO_3-Pt.

Figure 2 shows the XRD patterns of the prepared Co-OH-CO_3 and Co-OH-CO_3-Pt samples. There are characteristic diffraction peaks of Co-OH-CO_3 at 16.9°, 33.5°, and 34.8° which are assigned to the (020), (221), and (040) faces. The XRD patterns are consistent with the value in the standard card (JCPDS Card No. 048-0083). No other peaks of impurities are observed. The Co-OH-CO_3 NWs are rhombic oxide. The diffraction peaks at 39.7 °, 46.7°, 68.1°, and 81.9° are assigned to Pt (111), (200), (220), and (311) faces which indicates that the sputtered Pt catalysts are polycrystalline. Besides, the peaks of the stainless steel substrate are also detected.

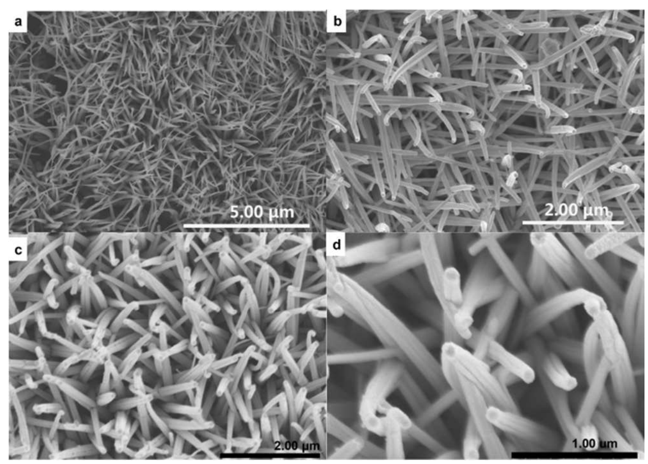

Figure 3 (a-b) FESEM images of the Co-OH-CO_3 NWs and Co-OH-CO_3-Pt electrode; (c-d) FESEM images of the Co-OH-CO_3-PdPt electrodes.

Figure 3a and 4a show the FESEM and TEM images of the Co-OH-CO_3 NWs. From the FESEM image, the Co-OH-CO_3 NWs were found directly grown on the stainless steel substrate. Gathered Co-OH-CO_3 NWs with a relatively high density are obviously observed. From the TEM image of Co-OH-CO_3 NWs in Figure 4a, each nanowire exhibits conical structure and the diameter is of around 80 nm at the bottom, the single nanowire is about 4 µm along the length direction.

Figure 3b-d and 4b-d show the morphologies of the Co-OH-CO_3-Pt and Co-OH-CO_3-PdPt electrodes. After sputtering deposition, the Co-OH-CO_3 NWs are decorated with catalysts. Along with the catalyst loading increasing, the conical structure has changed to the nanorods which can be found at Co-OH-CO_3-PdPt electrode (Fig 3c) clearly with areal number densities of 3 to 4 billion cm^{-2}.

From the TEM images of the electrodes in Figure 4b, the Co-OH-CO_3 NWs are decorated with 2~3 nm Pt catalysts after sputtering deposition. The deposited catalysts grow as thin films on oriented Co-OH-CO_3 NWs in Figure 4b-c. From the XRD analysis, the sputter deposited thin film catalysts display as polycrystalline layers. Along with the catalyst loading increasing, within the thin film catalysts, the oriented whiskerettes are formed on the Co-OH-CO_3 NWs sides. It can be seen that the catalyst whiskerettes oriented at an angle of about 68±2° w.r.t. the whisker axis, which is similar with the angle between the (111) crystal planes in cubic lattices, namely, 70.53°. According to the analysis in the SEM and TEM images of the Co-OH-CO_3-PdPt electrode, the Co-OH-CO_3-PdPt exhibits the "wheatear-like" structure in which catalyst whiskerettes could be taken as grains of wheat.

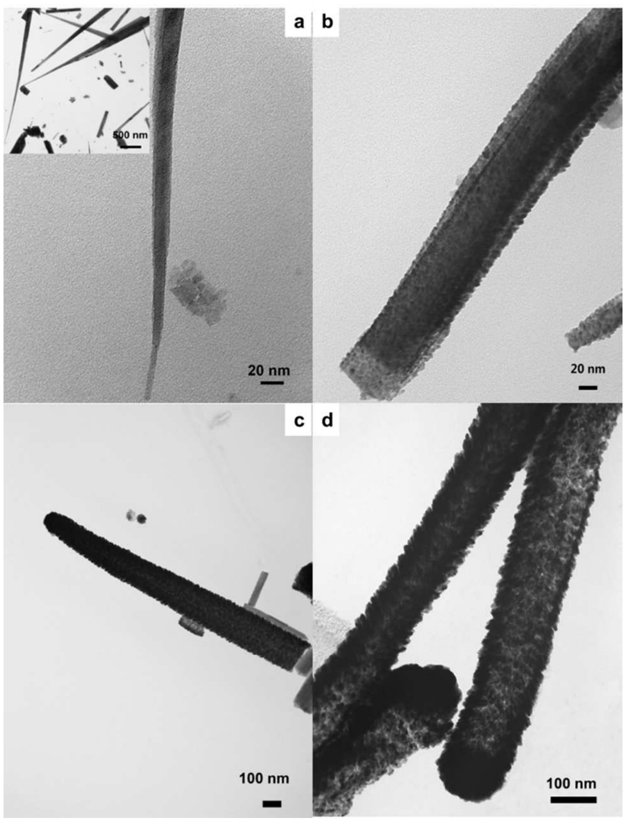

Figure 4 (a-c) TEM images of the Co-OH-CO_3 NWs, Co-OH-CO_3-Pt, and Co-OH-CO_3-PdPt; (d) TEM image of the Co-OH-CO_3-PdPt after acid leaching.

Figure 4d shows the TEM image of Co-OH-CO_3-PdPt electrode after acid leaching at 50mM H_2SO_4. It can be found that the Co-OH-CO_3 has been removed by acid, only <0.1% Co element could be test by the inductively coupled plasma atomic emission spectrometry (ICP-AES). The catalyst has changed to the hollow thin film structure that could be taken as transport of electron in CL. Figure 6 shows the SEM images of the prepared UTCL. The thickness of the prepared UTCL is about 300 nm.

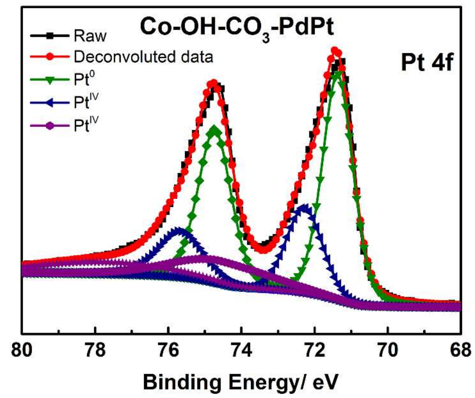

Figure 5 X-ray Photoelectron Spectroscopy (XPS) spectra for Pt 4f of the Co-OH-CO_3-PdPt.

Figure 5 shows the Pt 4f XPS spectra for the Co-OH-CO_3-PdPt electrode. The most intense peak (71.4 eV) of Pt $4f_{7/2}$ is assigned to metallic Pt (0). The second peak is assigned to Pt (II) as in PtO and $Pt(OH)_2$, and the third one is assigned to Pt (IV). The binding energy of Pt $4f_{7/2}$ for the Co-OH-CO_3-PdPt was slightly shifted to the positive direction in comparison with that of the referenced bulk Pt (0) (70.9 eV). The slightly shifted in the bulk metallic Pt (0) to higher binding energies may be attributed to a significant contribution from the interaction between Pt catalysts and support.

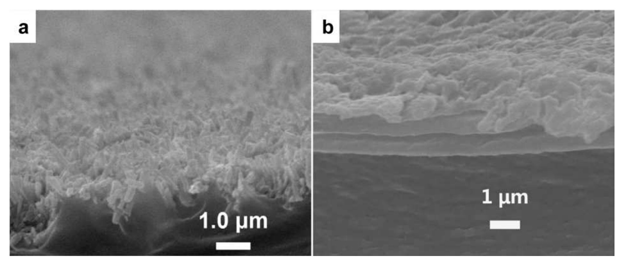

Figure 6 (a) SEM image of the Co-OH-CO_3-PdPt electrode after transferred onto Nafion®212 membrane; (b) SEM image of the UTCL based on Co-OH-CO_3-PdPt electrode.

The UTCL exhibits better performance than the CL without acid leaching procedure. In Figure S1, without acid leaching, the cell shows low performance, even after 10 mA cm^{-2} activation for 24h. On the other hand, the ionomer in the conventional CL serves as a binder and proton conductor, and it improved the catalyst utilization[24]. Nevertheless, the ionomer was skipped for the UTCL in this study. In addition, although there were no ionomer in the UTCL, the performance did not decrease because of the thin film catalysts and short diffusion pathway of the thinner CL.

Figure 7 shows the *I-V* curves of membrane electrode assembly (MEA) based on different UTCLs. The maximum power density of the different MEAs based on Co-OH-CO_3-Pt and Co-OH-CO_3-PdPt electrodes are 298 and 337 mW cm^{-2} respectively. According to the cyclic voltammetry (CV) curves of the MEAs (Figure S2), the electrochemical surface area (ECSA) of the catalysts are 54.6 $m^2\,g^{-1}_{Pt}$ for Co-OH-CO_3-Pt and 67.3 $m^2\,g^{-1}_{Pt+Pd}$ for Co-OH-CO_3-PdPt respectively.

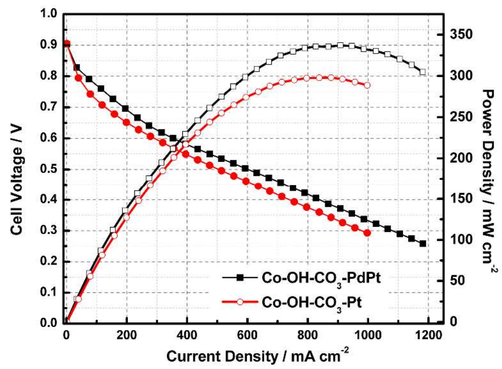

Figure 7 *I-V* curves of the UTCL based on Co-OH-CO_3-Pt and Co-OH-CO_3-PdPt electrodes.

(Testing condition: active area 1 cm^2, 65°C; gas flow rate of H_2/O_2 was 15/70 sccm min^{-1}; H_2/O_2 gases were externally humidified at dew point temperature of 65°C. Pt and Pd loading are 43 and 24 μg cm^{-2})

For comparison, the electrode with Pt catalysts sputtered onto gas diffusion layer (GDL) directly was also served as the anode and the cathode in a MEA. The SEM images of the GDL and GDL-Pt electrodes in Figure S3 show that deposited Pt catalysts in the diameter of around 60 nm aggregated on the GDL. Although the Pt loading at GDL-Pt is 0.12 mg cm^{-2} which is 2.8 times higher than at the Co-OH-CO_3-PdPt, the MEA based on GDL-Pt electrode has low performance, and the maximum power density is only 185 mW cm^{-2} shown in Figure S4. It is indicated that the MEAs based on the UTCL at ultra-low Pt loading exhibits enhanced performance.

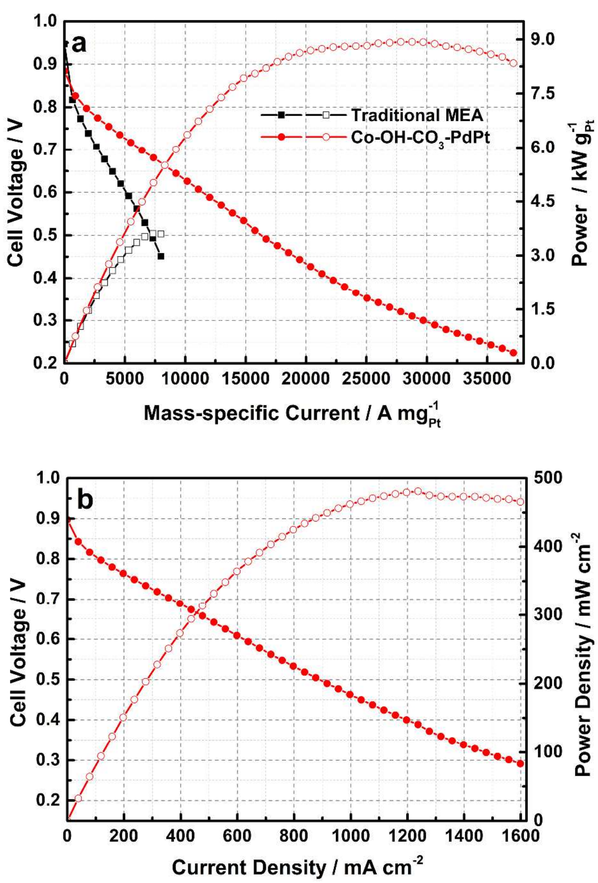

Figure 8 (a) *I-V* curves of the UTCL based on Co-OH-CO_3-PdPt electrode and traditional MEA at 0.05 MPa; (b) *I-V* curves of the UTCL based on Co-OH-CO_3-PdPt electrode at 0.1 MPa.

(Test condition: active area 5 cm^2, 65°C; the gas flow rate of H_2/O_2 was 60/200 sccm min^{-1}; H_2/O_2 gases were externally humidified at dew point temperature of 65°C, respectively. Pt and Pd loadings are 43 and 24 μg cm^{-2} for Co-OH-CO_3-PdPt electrode; Pt loading is 150 μg cm^{-2} for traditional MEA)

The performance of the novel UTCL was compared with the traditional MEA further. Figure 8a shows the *I-V* curves of the UTCL and traditional MEA. The maximum power of the UTCL can reach 8.9 kW g^{-1}_{Pt} which is about 2.5 times than the traditional MEA. Taking into account the meso-scale structure of the novel CL without any ionomer, it is suggested that ionomer might be not indispensable for the MEA with UTCL. The maximum power density of the UTCL is 481 mW cm^{-2} shown in Figure 8b corresponding to an overall specific power of 11.2 kW g^{-1}_{Pt}, which compares favourably to the performance of commercially available MEA.

Conclusions

In summary, an UTCL with oriented 3D wheatear-like structure catalysts was designed using the Co-OH-CO_3 NWs as template. Without ionomer as proton conductor, the fabricated UTCL exhibited enhanced performance at ultra-low Pt loading. The UTCL displayed a maximum power density of 481 mW cm^{-2} with Pt loading of 43 μg cm^{-2}_{Pt}, resulting in a relatively high Pt utilization of 11.2 kW g^{-1}_{Pt}. The results in this work provide convincing evidence that nanostructured thin film catalysts are promising for the application of fuel cells and other energy devices.

Experimental section

The synthesis of the Co-OH-CO_3 NWs was based on a hydrothermal method. The solution was prepared by dissolving 1.5 mM of $Co(NO_3)_2$, 3 mM NH_4F, and 7.5 mM of $CO(NH_2)_2$ in distilled water. Then this solution was transferred into Teflon-lined stainless steel autoclave linear. The stainless steel substrate was immersed into the reaction solution. The linear was sealed in a stainless steel autoclave and maintained at 120 °C for 5 h and then cooled to room temperature. The samples were collected and rinsed with distilled water several times.
The catalysts were deposited on Co-OH-CO_3 NWs using radio frequency (RF) sputtering method. The RF sputtering process was performed with a radio frequency magnetron sputtering system. During the sputtering process, the input power for the sputter cathode was 120 W and the Ar gas pressure was 0.8 Pa. For the Co-OH-CO_3-Pt electrode, the samples were subject to the Pt plasma directly. For the Co-OH-CO_3-PdPt electrode, Pd catalysts were firstly deposited onto the Co-OH-CO_3 NWs, and then deposit Pt catalysts. The loading of Pd and Pt are the same for all samples. For comparison, Pt nanoparticles were also deposited onto one side of gas diffusion layer (GDL) directly and the Pt loading is 0.12 mg cm^{-2}.
The electrodes were hot-pressed onto both sides of the Nafion® membrane. And then the UTCL were prepared by immersing the electrodes into 50 mM H_2SO_4 for 5h to remove Co-OH-CO_3. The

membrane electrode assembly (MEA) was pressed at 140^{o}C, 0.25 MPa for 1min. For the traditional MEA, 40% Pt/C catalysts (John Matthey, JM) were brushed onto GDL with Pt loading as 150 μg cm^{-2}, and the Nafion® ionomer loading is the same as carbon.

The morphology of the samples was characterized by field emission scanning electron microscope (FESEM, Hitachi S-4800) and Transmission electron microscopy (TEM, JEM2010-HR, 120 KV). The phase and the composition of the samples were investigated via X-ray diffraction (XRD, Bruker, D8 ADVANCE) with Cu Kα radiation (λ = 1.5418 Å). The catalysts loadings of the electrodes were measured by the inductively coupled plasma atomic emission spectrometry (ICP-AES) on Leeman Plasma-Spec-I equipment. X-ray Photoelectron Spectroscopy (XPS, Thermo Scientific ESCA Lab250 Xi spectrometer) with Al KR radiation in twin anode. For the XPS spectra, the binding energy was calibrated using the C 1s photoelectron peak at 284.6 eV as the reference.

During the fuel cell test, the cell temperature was 65^{o}C and the humidification temperature was 65/65^{o}C for H_2/O_2. KFM 2030 Impedance Meter (Kikusui, Japan) was used for the test of the *I-V* curves. The electrochemical surface area (ECSA) of the MEAs was evaluated by CV curves. Before CV measurement, the cathode of fuel cell purged by N_2 until the cell voltage is below 0.1 V. And the CV curves were measured at a scan rate of 50 mV s^{-1}.

Acknowledgements

This work was financially supported by the National Basic Research Program of China (973 program no. 2012CB215500), the National High Technology Research and Development Program of China (863 Program no. 2012AA052002), and the National Natural Science Foundations of China (no. 21176234, no. 2087614).

Notes and references

[a] Fuel Cell System and Engineering Laboratory, Dalian National Laboratory for Clean Energy, Dalian Institute of Chemical Physics, Chinese Academy of Sciences, 457 Zhongshan Road, Dalian 116023, PR China; E-mail: hmyu@dicp.ac.cn
[b] University of the Chinese Academy of Sciences, Beijing 100039, PR China

† Electronic Supplementary Information (ESI) available: [details of any supplementary information available should be included here]. See DOI: 10.1039/b000000x/

1. E. A. Ticianelli, C. R. Derouin, A. Redondo and S. Srinivasan, *J. Electrochem. Soc.*, 1988, 135, 2209.
2. W. Yuan, Y. Tang, X. Yang and Z. Wan, *Applied Energy*, 2012, 94, 309.
3. H. Zhang and P. K. Shen, *Chemical Reviews*, 2012, 112, 2780.
4. Z. Liu, L. Ma, J. Zhang, K. Hongsirikarn and J. G. Goodwin, *Catalysis Reviews*, 2013, 55, 255.
5. Z. Chen, M. Waje, W. Li and Y. Yan, *Angew. Chem. Int. Ed. Engl.*, 2007, 46, 4060.
6. H.-H. Li, C.-H. Cui, S. Zhao, H.-B. Yao, M.-R. Gao, F.-J. Fan and S.-H. Yu, *Adv. Energy Mater.*, 2012, 2, 1182.
7. C.-H. Cui, H.-H. Li and S.-H. Yu, *Chem. Sci*, 2011, 2, 1611.
8. A. Ohma, T. Mashio, K. Sato, H. Iden, Y. Ono, K. Sakai, K. Akizuki, S. Takaichi and K. Shinohara, *Electrochimica Acta*, 2011, 56, 10832.
9. M. K. Debe, *J Electrochem Soc*, 2013, 160, F522.
10. M.K.Debe, *Handbook of fuel cell*, 2003, 3, 576.
11. E. Middelman, *Fuel Cells Bulletin*, 2002, 2002, 9.
12. Z. Q. Tian, S. H. Lim, C. K. Poh, Z. Tang, Z. Xia, Z. Luo, P. K. Shen, D. Chua, Y. P. Feng, Z. Shen and J. Lin, *Adv. Energy Mater.*, 2011, 1, 1205.
13. W. Zhang, A. I. Minett, M. Gao, J. Zhao, J. M. Razal, G. G. Wallace, T. Romeo and J. Chen, *Adv. Energy Mater.*, 2011, 1, 671.
14. W. Zhang, J. Chen, A. I. Minett, G. F. Swiegers, C. O. Too and G. G. Wallace, *Chem. Commun.*, 2010, 46, 4824.
15. M. S. Saha, R. Li, M. Cai and X. Sun, *J Power Sources*, 2008, 185, 1079.
16. C. Zhang, H. Yu, Y. Li, Y. Gao, Y. Zhao, W. Song, Z. Shao and B. Yi, *ChemSusChem*, 2013, 6, 659.
17. C. Zhang, H. Yu, Y. Li, W. Song, B. Yi and Z. Shao, *Electrochim. Acta*, 2012, 80, 1.
18. C. Zhang, H. Yu, Y. Li, L. Fu, Y. Gao, W. Song, Z. Shao and B. Yi, *Nanoscale*, 2013, 5, 6834.
19. Z. X. Xia, S. L. Wang, Y. J. Li, L. H. Jiang, H. Sun, S. Zhu, D. S. Su and G. Q. Sun, *Journal of Materials Chemistry A*, 2013, 1, 491.
20. J. Jiang, J. Liu, R. Ding, J. Zhu, Y. Li, A. Hu, X. Li and X. Huang, *ACS Appl Mater Interfaces*, 2011, 3, 99.
21. X. Xia, J. Tu, Y. Zhang, X. Wang, C. Gu, X. Zhao and H. Fan, *ACS Nano*, 2012, 6, 5531.
22. X. Xia, J. Tu, Y. Zhang, J. Chen, X. Wang, C. Gu, C. Guan, J. Luo and H. J. Fan, *Chem. Mater.*, 2012, 24, 3793.
23. J. Jiang, J. P. Liu, X. T. Huang, Y. Y. Li, R. M. Ding, X. X. Ji, Y. Y. Hu, Q. B. Chi and Z. H. Zhu, *Crystal Growth & Design*, 2010, 10, 70.
24. S. G. M. S. WILSON, *J. Appl. Electrochem.*, 1992, 22, 7.